Improving the *sd*-shell effective interaction obtained from the Daejeon16 nucleon-nucleon interaction

Ik Jae Shin,[1,*] Nadezda A. Smirnova,[2,†] Andrey M. Shirokov,[3,‡] Zuxing Yang,[4,5,§] Bruce R. Barrett,[6] Zhen Li,[2,‖] Youngman Kim,[7,¶] Pieter Maris,[8,**] and James P. Vary[8,††]

[1]*Institute for Rare Isotope Science, Institute for Basis Science, Daejeon 34000, Republic of Korea*
[2]*LP2IB (CNRS/IN2P3–Université de Bordeaux), 33175 Gradignan Cedex, France*
[3]*Skobeltsyn Institute of Nuclear Physics, Lomonosov Moscow State University, 119991 Moscow, Russia*
[4]*Institute of Modern Physics, Chinese Academy of Science, Lanzhou, Gansu 730000, People's Republic of China*
[5]*RIKEN Nishina Center, Wako, Saitama 351-0198, Japan*
[6]*Department of Physics, University of Arizona, Tucson, Arizona 85721, USA*
[7]*Center for Exotic Nuclear Studies, Institute for Basic Science, Daejeon 34126, Republic of Korea*
[8]*Department of Physics and Astronomy, Iowa State University, Ames, Iowa 50011, USA*

(Received 29 June 2023; accepted 31 July 2024; published 9 September 2024)

We present new microscopic effective shell-model interactions in the valence *sd* shell, obtained from the modern Daejeon16 nucleon-nucleon potential using no-core shell-model (NCSM) wave functions of ^{18}F at $N_{\max} = 6$ (total oscillator quanta of excitation) model space and the Okubo-Lee-Suzuki transformation. First, we explore the convergence properties of our calculations and show that the excitation energies of states in ^{18}F, characterized by the largest valence-like configurations, are reasonably converged and the lowest states are in sensible agreement with experiment. Then, we investigate the monopole properties of that interaction in comparison with the phenomenological universal *sd*-shell interaction, USDB, and with the previously derived interaction at $N_{\max} = 4$. Theoretical binding energies and low-energy spectra of the O isotopes, as well as low-energy spectra of a selection of *sd*-shell nuclei, are presented. We conclude that the use of larger-space NCSM wave functions leads to a noticeable improvement in the quality of the derived effective interaction. We propose monopole modifications of the Daejeon16 centroids which further improve the agreement with experiment throughout the *sd* shell, as demonstrated by a compilation of spectra contained in Supplemental Material.

DOI: 10.1103/PhysRevC.110.034306

I. INTRODUCTION

The last decade has seen new approaches to the long-standing nuclear-structure problem of the construction of effective model-space interactions. Among them are advanced applications of the many-body perturbation theory [1–4], as well as recently developed nonperturbative approaches based on the similarity-renormalization group (SRG) concept and known as in-medium SRG (IMSRG) [5–7], coupled-cluster theory [8], and an approach based on the Okubo-Lee-Suzuki (OLS) transformation of no-core shell-model (NCSM) wave functions [9–12]. Many of these approaches have introduced explicitly the three-nucleon forces [2–8], improving the monopole term of the corresponding interactions to get closer to the successful phenomenological interactions such as USD and USDB [13,14] in the *sd* shell or KB3G [15] and GXPF1A [16] in the *pf* shell. All these are important steps towards *ab initio* theory of atomic nuclei.

In this article we present our progress along the lines reported in Ref. [12], where an effective interaction for the *sd* shell-model space was constructed based on the NCSM results using various nucleon-nucleon potentials. In that work the NCSM calculations were performed for ^{18}F, as well as for ^{16,17}O and ^{17}F in the model space defined by maximal total oscillator quanta of excitation $N_{\max} = 4$. For the oscillator parameter of the single-particle basis, $\hbar\Omega = 14$ MeV was chosen. The unitary OLS transformation was exploited to reduce the Hamiltonian to a block-diagonal form, separating the model space (*sd* shell) from the rest. Subtraction of the NCSM core energy and one-body contributions generated a set of 63 two-body matrix elements (TBMEs), defining a residual two-body interaction in the *sd*-shell valence space. Among different high-precision potentials employed, such as chiral N3LO (from Ref. [17]), JISP16 [18], and Daejeon16 [19], the best agreement with experiment for selected *sd*-shell nuclei was achieved for Daejeon16. It was also shown that the

*Contact author: geniean@ibs.re.kr
†Contact author: nadezda.smirnova@u-bordeaux.fr
‡Contact author: shirokov@nucl-th.sinp.msu.ru
§Contact author: zuxing.yang@riken.jp
‖Contact author: zli@theorie.ikp.physik.tu-darmstadt.de
¶Contact author: ykim@ibs.re.kr
**Contact author: pmaris@iastate.edu
††Contact author: jvary@iastate.edu

effective valence-space interaction derived from the Daejeon16 with the correction to the monopole part resulted in a very good description of O binding energies and showed improved description of spectra. This conclusion was supported by the study of upper *sd*-shell nuclei which have been investigated in Ref. [20], using the same interactions. In addition, in Ref. [21] we have initiated construction of effective electromagnetic operators for valence-space calculations with effective interactions originating from Daejeon16.

In the present study, we again employ the Daejeon16 interaction and construct an *sd*-shell effective interaction now based on $N_{\max} = 6$ NCSM results. The results are compared with the previously derived interaction at $N_{\max} = 4$ and with the phenomenological USDB interaction.

The paper is organized as follows. After a brief introduction to the method of deriving the effective valence-space interactions, we discuss the convergence properties of our calculations, as well as explain the challenges in the state selection, which provides support for our choice of the oscillator parameter. Then, we present the resulting valence space interaction, DJ16$_6$, obtained from the Daejeon16 *NN* potential at $N_{\max} = 6$ and compare it with the previously derived interaction at $N_{\max} = 4$, DJ16$_4$. In particular, we discuss the properties of two-body centroids which describe a spherical mean field and are important bellwethers for nuclear spectroscopy. The main part of the article demonstrates the comparison of the low-lying spectra and binding energies of the O isotopes to illustrate the $T = 1$ component. Then, we discuss the spectra of the odd-A F isotopes and ^{39}K to understand the main features of the proton-neutron centroids. We also test the interaction on some selected *sd* shell nuclei. We then perform some minimal modifications of the mainly $T = 1$ centroids of the effective interaction DJ16$_6$ in order to improve the agreement with the experimental data. The extensive calculation of spectra of *sd* shell nuclei are presented in Supplemental Material [22]. We conclude with our summary and outlook.

II. MICROSCOPIC TWO-BODY INTERACTIONS: FORMALISM, CONVERGENCE, AND STATE SELECTION

The derivation of the effective valence-space interaction has been discussed in detail in Refs. [9–12]. We start with a translationally-invariant Hamiltonian for A pointlike nucleons interacting via a realistic *NN* interaction

$$H = \sum_{i}^{A} \frac{\vec{p}_i^{\,2}}{2m} - \frac{\vec{P}^2}{2mA} + \sum_{i<j}^{A} V_{ij}^{NN}, \tag{1}$$

where m is the nucleon mass (approximated here as the average of the neutron and proton mass), $\vec{p}_i$ are nucleonic momenta, $\vec{P} = \sum_{i=1}^{A} \vec{p}_i$, and V_{ij}^{NN} denotes the *NN* interaction. The two-body Coulomb interaction is included between the protons. We do not include three-nucleon ($3N$) forces, because we use the Daejeon16 nucleon-nucleon potential which provides a good description of light nuclei without $3N$ interaction due to the fact that its off-shell properties were adjusted by using phase-equivalent transformations to take effectively three-nucleon and other many-nucleon interactions into account.

Within the NCSM, the eigenproblem for H is solved by diagonalizing the Hamiltonian matrix in a many-body spherical harmonic-oscillator (HO) basis. The model space is defined by two parameters: (i) by a given HO energy quantum, $\hbar\Omega$, and (ii) by a cutoff in the total number of the HO excitation quanta, $N_{\max}$. This means that we retain only many-body configurations, satisfying the condition $N_{\min} \leqslant \sum_{i=1}^{A}(2n_i + l_i) = N_{\min} + N \leqslant N_{\min} + N_{\max}$, where n_i is the single-particle radial HO quantum number, l_i is the single-particle orbital angular momentum quantum number, while $N_{\min}$ is the minimum of the summation that satisfies the Pauli principle for the chosen A-nucleon system. Consequently, $N = 0, \ldots, N_{\max}$.

One of the important advantages of the HO basis is that it allows one to separate the spurious center-of-mass motion. In practice, a truncation by the total number of HO quanta in the many body system leads to an exact factorization of the center-of-mass wave function and the intrinsic wave function; adding a center-of-mass term $\beta(H_{CM} - \frac{3}{2}\hbar\Omega)$ to the Hamiltonian (1) shifts states with center-of-mass excitations by $\beta\hbar\Omega$ [23].

In the present study, we perform the NCSM calculations using the bare Daejeon16 *NN* potential. That is, we omit the first OLS renormalization, previously performed at the two-nucleon cluster level [12], since Daejeon16 is reasonably soft and calculations in $N_{\max} = 6$ basis spaces are close enough to convergence for our purposes. As a starting point, we calculate the ground state energy and the spectra of ^{16}O, ^{17}O, ^{17}F, and ^{18}F at a set of $\hbar\Omega$ values ranging from 12 to 26 MeV, using a highly parallelized Multi-Fermion Dynamics for nuclei (MFDn) code [24–28].

The microscopic effective interactions obtained from NCSM depend on $N_{\max}$ and $\hbar\Omega$. On the other hand, the eigenvalues of the bound states of the NCSM results converge as $N_{\max}$ increases towards results independent of $\hbar\Omega$ and $N_{\max}$ [29]. The ground state energies of oxygen isotopes with $A = 16, 18$ and the energy of the lowest $5/2^+$ state of ^{17}O are shown in Fig. 1 as functions of $\hbar\Omega$ for $N_{\max} = 0, 2, 4, 6, 8$. We also present the extrapolated values obtained following the "extrapolation B" procedure of Ref. [30]. First, we remark that Daejeon16, being a soft potential, results in a rather rapid convergence for these states. Second, we note that for all nuclei we obtain a slight overbinding as compared to experiment. The minimum energy is attained near $\hbar\Omega = 18$ MeV, which is also the case for excited states (not shown in this figure).

Although the largest model space for which NCSM calculations are feasible for $A = 18$ is the one defined by $N_{\max} = 8$, to construct an effective interaction we need to identify the required 28 NCSM eigenstates. It turns out that the states 0_3^+, 2_5^+, $T = 1$ and 1_5^+, 3_2^+, $T = 0$ are shifted higher in energy and appear in a region of dense NCSM solutions, with increasing $\hbar\Omega$. This phenomenon is illustrated in Fig. 2 for $N_{\max} = 4$ calculations for 0^+ and 2^+ in ^{18}O and for 1^+, $T = 0$ states in ^{18}F (without Coulomb interaction for clarity of presentation). For example, at $\hbar\Omega = 12$ MeV, the three lowest 0^+, $T = 1$ states and five lowest 2^+, $T = 1$ states are the states which carry the largest $N = 0$ components among all the states of the

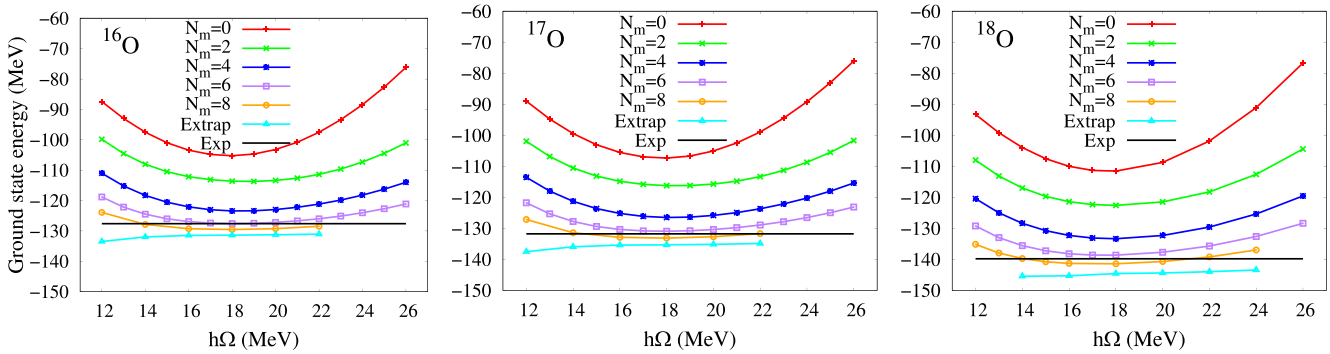

FIG. 1. Ground-state energies of ^{16,18}O and the lowest $5/2^+$ state energy of ^{17}O obtained within the NCSM from the Daejeon16 *NN* potential in comparison with experiment.

same J^π, T quantum numbers. However, already at $\hbar\Omega = 14$ MeV, because of the (avoided) level crossing, 0^+_3 becomes an intruder state and it is 0^+_4 which is selected for the OLS transformation (see left panel of Fig. 2). Similarly, at $\hbar\Omega = 14$ MeV we chose 2^+_6 as a fifth 2^+, $T = 1$ state for the OLS transformation as evident from the middle panel of Fig. 2. The situation with 1^+ and 3^+, $T = 0$ states is even more complicated: these states rapidly go up in energy and penetrate into a region of the high level density. The twelve lowest 1^+, $T = 0$ states in ^{18}F are shown in the right panel of Fig. 2. Besides the four lowest states, it is the ninth 1^+, $T = 0$ state which is included for the construction of the *sd*-shell interaction.

The above-described situation becomes more complicated at $N_{\max} = 6$. Thus, we require a large number of converged states. Their identification becomes more difficult due to numerous (avoided) level crossings and fractioning of the states. In general, there is a good continuity of the values of TBMEs derived as a function of $N_{\max}$ and of $\hbar\Omega$ up to $\hbar\Omega = 18$ MeV, where more serious ambiguities in the state selection enter. Aiming at stable results, we thus limit ourselves to the $N_{\max} = 6$ model space and, following the previous studies [11,12], we derive the effective interaction at $\hbar\Omega = 14$ MeV. This value is close to the empirical shell-model value for ^{16}O [31]. The selected 28 eigenstates of ^{18}F characterized by the largest contribution of $N = 0$ components at $\hbar\Omega = 14$ MeV and $N_{\max} = 6$ (see Table I, left part) in comparison with the states selected in our previous work at $N_{\max} = 4$ (right part of the Table). These states have been used to set up the OLS transformation to the *sd*-shell valence space. Although the $N = 0$ component of the 0^+_3, 2^+_5, $T = 1$ and 1^+_5, 3^+_2, $T = 0$ states in ^{18}F is falling below 30%, we are able to clearly identify them among a set of states with even smaller components in the valence space. The probability of the $N = 0$ component, denoted as $\alpha^2_{N=0}$, is given for each selected state in Table I. We checked that the use of $\hbar\Omega = 16$ and 18 MeV does not bring any qualitative improvement to the interactions, but complicates the construction because of the problems indicated above.

To illustrate the convergence of our calculations, we show in Fig. 3 the excited states of ^{18}F, characterized by the largest $N = 0$ components, as a function of $N_{\max}$. Indeed, the majority of the states stay relatively constant in energy. Only the highest 0^+ and 2^+ $T = 1$ states and the highest 1^+ and 3^+ $T = 0$ states, containing lower contribution of $N = 0$ components, show a decrease in energy when moving from $N_{\max} = 4$ to $N_{\max} = 6$. The other states are reasonably converged. We also remark that the absolute values of $N = 0$ components reduce at $N_{\max} = 6$ as compared to those obtained at to $N_{\max} = 4$. This is a consequence of the increase of the model space.

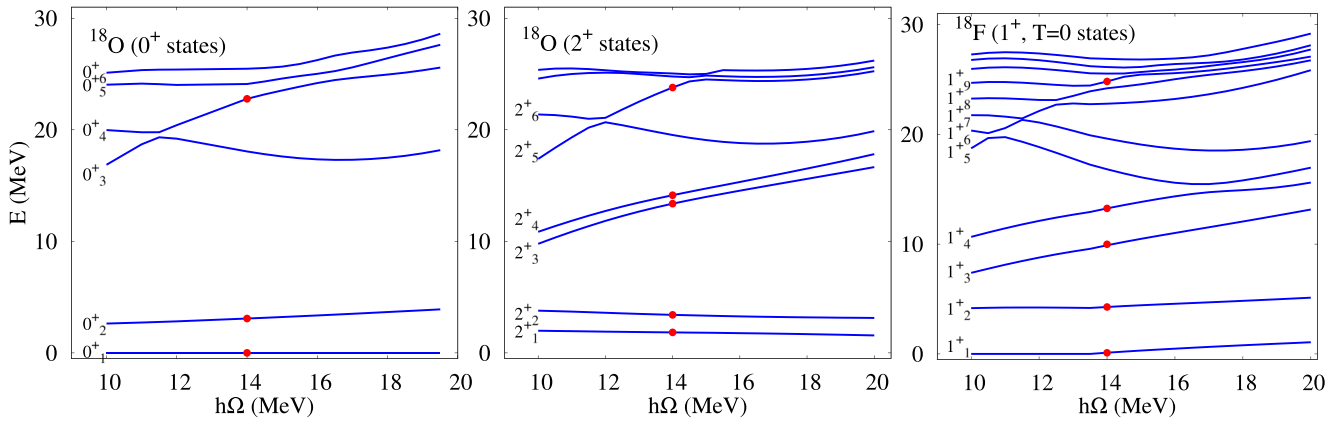

FIG. 2. Evolution of 0^+ and 2^+ states in ^{18}O and 1^+, $T = 0$ states in ^{18}F, obtained within the NCSM with the Daejeon16 *NN* potential at $N_{\max} = 4$ as a function of $\hbar\Omega$. For illustration purpose, the calculation of ^{18}F was done without Coulomb interaction to avoid isospin mixing. The states, labeled by red dots, are those having largest $N = 0$ components at $\hbar\Omega = 14$ MeV. See text for detail.

TABLE I. The NCSM energies (in MeV) of the lowest 28 states J_i^π of ^{18}F calculated in the $N_{\max} = 6$ model space (left) and $N_{\max} = 4$ model space (right) using the Daejeon16 *NN* interaction with $\hbar\Omega = 14$ MeV. These are states which contain the largest $N = 0$ components (reported in the column $\alpha^2_{N=0}$), and therefore are chosen for the OLS transformation to the valence space ($N'_{\max} = 0$).

J_i^π	T	$N_{\max} = 6$	$\alpha^2_{N=0}$	J_i^π	T	$N_{\max} = 4$	$\alpha^2_{N=0}$
1^+_1	0	−133.311	0.583	3^+_1	0	−126.069	0.675
3^+_1	0	−133.191	0.600	1^+_1	0	−126.032	0.668
0^+_1	1	−132.017	0.583	5^+_1	0	−125.087	0.694
5^+_1	0	−131.991	0.619	0^+_1	1	−124.817	0.670
2^+_1	0	−130.288	0.588	2^+_1	0	−123.081	0.672
2^+_2	1	−130.028	0.597	2^+_2	1	−122.965	0.679
1^+_2	0	−129.016	0.602	1^+_2	0	−121.884	0.684
0^+_2	1	−128.837	0.602	0^+_2	1	−121.778	0.682
2^+_3	1	−128.316	0.616	2^+_3	1	−121.402	0.691
4^+_1	1	−127.909	0.625	4^+_1	1	−121.071	0.700
3^+_2	0	−127.624	0.609	3^+_2	0	−120.591	0.690
3^+_3	1	−127.443	0.604	3^+_3	1	−120.421	0.684
1^+_3	0	−124.407	0.528	1^+_3	0	−116.545	0.640
4^+_2	0	−122.693	0.572	4^+_2	0	−115.164	0.668
2^+_4	0	−122.255	0.481	2^+_4	0	−114.521	0.656
1^+_4	0	−121.000	0.508	1^+_4	0	−113.214	0.632
4^+_3	1	−119.817	0.568	4^+_3	1	−112.337	0.671
2^+_5	1	−119.401	0.510	2^+_5	1	−111.594	0.651
3^+_4	0	−119.281	0.546	3^+_4	0	−111.579	0.658
2^+_6	0	−119.018	0.526	1^+_5	1	−111.112	0.660
1^+_5	1	−118.766	0.551	2^+_6	0	−111.092	0.638
2^+_7	1	−118.483	0.551	2^+_7	1	−110.803	0.651
1^+_6	1	−118.381	0.560	1^+_6	1	−110.779	0.658
3^+_5	1	−118.205	0.572	3^+_5	1	−110.748	0.673
3^+_6	0	−112.705	0.280	3^+_6	0	−103.869	0.588
0^+_3	1	−110.598	0.172	0^+_3	1	−102.246	0.454
1^+_7	0	−109.812	0.193	1^+_7	0	−101.928	0.330
2^+_8	1	−109.495	0.279	2^+_8	1	−101.291	0.598

Performing the OLS transformation, the effective valence Hamiltonian, $H_{18}^{P'}$, an effective one- and two-body operator for $N'_{\max} = 0$, is derived (here prime is used to denote the valence space as in the previous works [11,12]). By construction, the energies of $H_{18}^{P'}$ for two valence nucleons in the *sd* shell exactly coincide with the selected eigenvalues of NCSM Hamiltonian for ^{18}F in the full $N_{\max} = 6$ oscillator space. See Ref. [11] for more details.

A NCSM calculation with the same $N_{\max} = 6$ and $\hbar\Omega = 14$ MeV is performed for ^{16}O to get the core energy and for ^{17}O and ^{17}F. Subtracting the core energy from the latter calculations, one obtains effective neutron and proton one-body terms. Subtraction of the core energy plus the one-body terms from the effective Hamiltonian for ^{18}F allows one to obtain the residual TBMEs to be used in the valence-space shell-model calculations. The core energy and the single-particle energies obtained from the Daejeon16 *NN* potential are given in

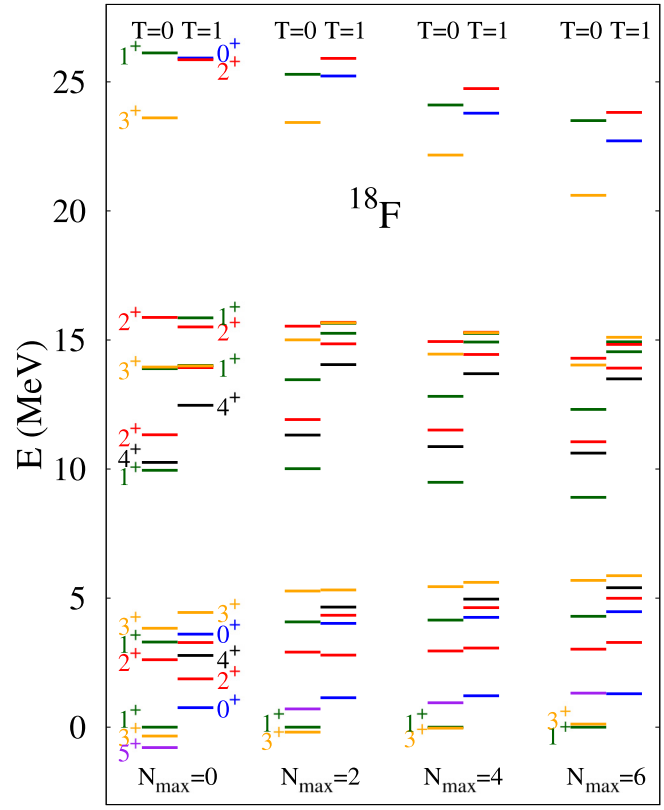

FIG. 3. Excitation spectrum of twenty-eight states having the largest $N = 0$ component in ^{18}F as obtained within the NCSM from the Daejeon16 *NN* potential at $\hbar\Omega = 14$ MeV. The energies are indicated relative to the position of the lowest ($1^+, T = 0$) state, since it is the known ground state spin and parity of ^{18}F. $T = 0$ states are shown on the left, while the $T = 1$ spectrum is on the right of each $N_{\max}$ column.

Table II ($N_{\max} = 6$ results in comparison with $N_{\max} = 4$ results), while the $N_{\max} = 6$ TBMEs are summarized in Table I of the Supplemental Material [22]. The text files with TBMEs are also available online [32].

In general, performing similar transformations on a three-valence nucleon system (^{19}F), one can get effective 3*N* matrix elements in the valence space. However, it was shown in Ref. [11] that the spectrum of ^{19}F obtained in the *sd* shell with the valence effective two-nucleon interactions only is almost identical to the spectrum obtained from the NCSM. This signifies that the role of effective 3*N* interactions appears to be small. In this work we consider only two-nucleon

TABLE II. Neutron ("ν") and proton ("π") single-particle energies (in MeV) obtained from the bare Daejeon16 potential for $A = 17$ at $N_{\max} = 6$ (left) and $N_{\max} = 4$ (right) for $\hbar\Omega = 14$ MeV.

	$N_{\max} = 6$			$N_{\max} = 4$		
	$E_{\rm core} = -124.485$			$E_{\rm core} = -118.307$		
(nlj)	$1s_{1/2}$	$0d_{5/2}$	$0d_{3/2}$	$1s_{1/2}$	$0d_{5/2}$	$0d_{3/2}$
$\epsilon_\nu(nlj)$	−3.697	−3.299	5.823	−3.115	−2.953	6.889
$\epsilon_\pi(nlj)$	−0.253	0.290	9.063	0.362	0.621	10.174

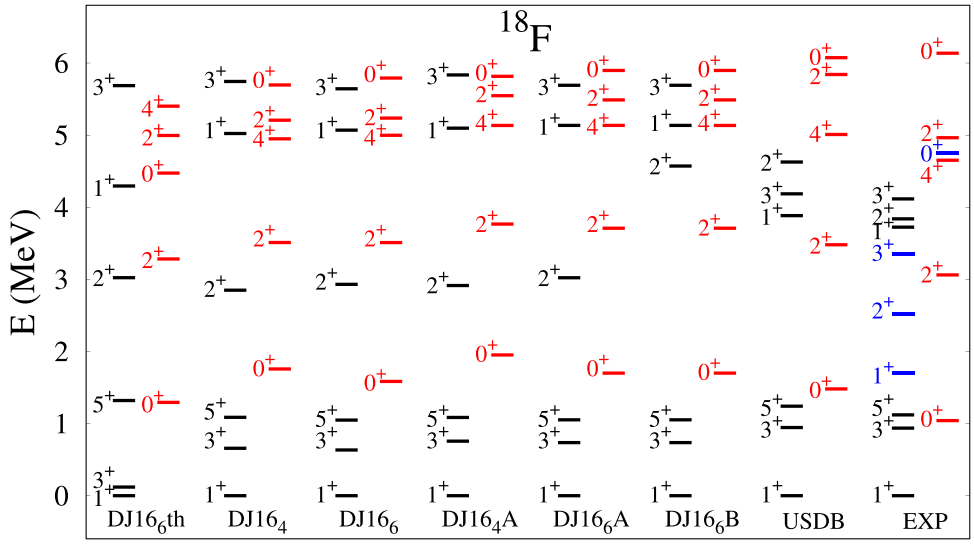

FIG. 4. Low-energy spectra (six lowest $T = 0$ states in black and five lowest $T = 1$ states in red) of ^{18}F obtained from USDB and from the microscopic effective interactions derived using Daejeon16 in comparison with experiment. For DJ16$_6$th, the isospin symmetry is approximate. In the experimental spectrum we indicate additional possible low-energy intruder states (in blue color): (1^+_2, 2^+_1, 3^+_2, $T = 0$) and (0^+_2, $T = 1$), which should not be compared with results from *sd*-shell theory. The USDB single-particle energies have been used in all calculations except for DJ16$_6$th, which is the NCSM spectrum at $N_{\max} = 6$ and $\hbar\Omega = 14$ MeV. DJ16$_4$A is a monopole-modified version of DJ16$_4$, while DJ16$_6$A and DJ16$_4$B are modified versions of DJ16$_6$ (see following sections).

interactions in the valence space. As is evident from Table II, theoretical single-particle energies obtained at $N_{\max} = 6$ are qualitatively similar to those obtained at $N_{\max} = 4$ to within an overall shift, and therefore they are also very different from the best empirical values as set by the USDB Hamiltonian: $\varepsilon(0d_{5/2}) = -3.9257$ MeV, $\varepsilon(1s_{1/2}) = -3.2079$ MeV, and $\varepsilon(0d_{3/2}) = 2.1117$ MeV. First, the $d_{5/2}$ and $s_{1/2}$ orbitals remain inverted. Second, the spin-orbit splitting between $d_{3/2}$ and $d_{5/2}$, being about 9 MeV at $N_{\max} = 6$, is still much larger than the empirical value of about 6.0 MeV. These deficiencies in single-particle energies lead to similar problems with the description of nuclear spectra and binding energies, as was discussed in Ref. [12]. While we plan to further investigate the theoretical single-particle energies in the future, in the present study we limit ourselves to the comparison of the TBMEs and, therefore, we adopt the USDB single-particle energies which are the same for neutrons and protons for our valence space calculations that compare theory with experiment.

Figure 4 shows the low-energy spectrum of ^{18}F obtained from USDB and from various microscopic effective interactions obtained from Daejeon16 as well as the experimental spectrum. The first column, DJ16$_6$th, shows the theoretical spectrum from the NCSM at $N_{\max} = 6$ (Table I). The same spectrum is reproduced from the effective *sd*-shell interaction with theoretical single-particle energies given in Table II. The interactions named DJ16$_4$ and DJ16$_4$A are those obtained from the NCSM calculations at $N_{\max} = 4$: the original and the monopole-modified, respectively, which have been thoroughly investigated in Ref. [12] (in that work they were denoted as DJ16 and DJ16A, respectively). We recall that DJ16$_4$ was obtained from the NCSM calculation with OLS-transformed two-nucleon Hamiltonian. The resulting TBMEs, as well as O binding energies and excitation spectra of studied nuclei are very close to those obtained from the NCSM with the bare Daejeon16 potentials without the OLS renormalization. Therefore, it is reasonable to use the published results with DJ16$_4$ for comparison in the present study. The interaction named DJ16$_6$ is obtained by the NCSM calculations with Daejeon16 at $N_{\max} = 6$ in the present work, while DJ16$_6$A and DJ16$_6$B are two phenomenologically modified versions of DJ16$_6$, as will be explained in the following sections. All calculations, except for DJ16$_6$th, employ the USDB single-particle energies and, therefore, the states are characterized by a given total isospin quantum number. In the case of DJ16$_6$th, the isospin symmetry is approximate.

In general, we notice a reasonable agreement between all theoretical spectra shown in Fig. 4 and the experimental data. All interactions predict correct spin and parities of the ground and the first excited state. We notice that the $T = 1$ band lies higher than experiment. Also, in the five theoretical spectra (counting from the left), 2^+_1, $T = 0$ appears to be too low, while 1^+_2 and 3^+_2, $T = 0$, appear to be too high. The former feature is improved by DJ16$_6$B, since we have modified a few nondiagonal ($J = 2, T = 0$) TBMEs. We did not make any attempts to correct for the position of the 1^+_2 or 3^+_2, $T = 0$ states. The phenomenological USDB Hamiltonian well describes these particular spectral features.

In the present study, to adopt the derived TBMEs through the *sd* shell, we use the same phenomenological A dependence as previously, namely, the $(A/A_0)^{-0.3}$ scaling ($A_0 = 18$) used also with USDB [14]. In theory, A dependence would arise from the many-body effective interactions derivable within the OLS procedures, which is beyond the scope of the present work. The single-particle energies are kept constant for all calculations.

III. MONOPOLE PROPERTIES

We initiate our analysis of the quality of our derived valence-space interactions from a study of their monopole component. The monopole part [33] of the valence-space shell-model Hamiltonian plays an important role for spectroscopic properties since it encapsulates the robust evolution of the spherical nuclear mean field as a function of valence nucleons [34,35]. A very useful insight is provided by the so-called *effective single-particle energies (ESPEs)* [36,37]. Assuming a normal filling of the single-particle orbitals as could be obtained from a pure monopole Hamiltonian, we evaluate ESPEs for a closed subshell nucleus (A) with respect to a reference nucleus (A_r) according to the expression

$$\tilde{\varepsilon}_k^{\rho}(A) = \varepsilon_k^{\rho}(A_r) + \sum_{k',\rho'} V_{kk'}^{\rho\rho'}(A)\, n_{k'}^{\rho'}. \tag{2}$$

Here, k (k') refer to a complete set of quantum numbers of a harmonic oscillator orbital, e.g., $k \equiv (n_k l_k j_k)$, k' runs over valence space orbitals beyond A_r, and $n_{k'}^{\rho'}$ is the occupation number of the orbital k' for nucleons of the type ρ'. The quantities $V_{kk'}^{\rho\rho'}$ are centroids of the two-body interaction,

$$V_{kk'}^{\rho\rho'} = \frac{\sum_J \langle k_\rho k'_{\rho'}|V|k_\rho k'_{\rho'}\rangle_J (2J+1)}{\sum_J (2J+1)}, \tag{3}$$

where ρ, ρ' denote protons (π) or neutrons (ν) and the total angular momentum of a two-body state J runs over all values allowed by the Pauli principle. Since the TBMEs $\langle k_\rho k'_{\rho'}|V|k_\rho k'_{\rho'}\rangle_J$ do not depend on the total angular momentum projection M, we skip it in the notation. The $T = 1$ and $T = 0$ centroids ($V_{kk'}^{T=0,1}$) can be obtained via the same equation, but using either $T = 1$ or $T = 0$ TBMEs in the summation.

The monopole part of the Hamiltonian describes a *spherical nuclear mean field*, which plays a lead role in the filling of orbitals and establishing (sub) shell gaps. Its single-particle states, or ESPEs, provide an important ingredient for the arrangement of shells and the interplay between spherical and deformed configurations in nuclei. The higher multipole part of the interaction provides the so-called *correlation energy* for particle-hole excitations across the shell gap. Large shell gaps are a prerequisite for magic numbers. A reduction of the spherical shell gaps may lead to a deformed ground state, if the correlation energy of a given excited (intruder) configuration is large enough to overcome the naive cost in energy for producing the excited configuration.

It has been recognized [34] that the main defect of the traditional microscopic effective interactions derived from two-body NN potentials is an unsatisfactory monopole term, resulting in the absence of sufficiently large subshell gaps and providing overbinding of systems beyond traditional closed-shell nuclei. This in turn leads to the lack of sphericity in closed subshell nuclei and failures in the description of open-shell nuclei. Given the importance of the monopole component of an effective interaction, we now provide a detailed analysis of the ESPEs of the valence-space interactions under consideration here.

TABLE III. Evolution of the $N = 14$ subshell gap and neutron $d_{5/2}$-$d_{3/2}$ spin-orbit splitting in the O isotopes from ^{16}O to ^{28}O as obtained from the ESPEs of different Hamiltonians.

	Gap $\nu(s_{1/2}-d_{5/2})$ (MeV)				Gap $\nu(d_{3/2}-d_{5/2})$ (MeV)			
	^{16}O	^{22}O	^{24}O	^{28}O	^{16}O	^{22}O	^{24}O	^{28}O
DJ16$_4$	0.72	2.21	0.88	1.98	6.04	6.08	6.18	7.11
DJ16$_6$	0.72	2.56	1.13	1.87	6.04	6.45	6.36	7.18
DJ16$_4$A	0.72	3.78	1.80	2.51	6.04	7.37	7.15	7.02
DJ16$_6$A	0.72	3.75	1.89	2.20	6.04	7.52	7.16	6.97
USDB	0.72	3.75	2.09	2.99	6.04	7.53	7.49	7.28

To illustrate the properties of the $T = 1$ centroids of the microscopic effective interactions in comparison with those of the phenomenological USDB interaction, we show in Figs. 5(a)–5(e) the neutron ESPEs in O isotopes with closed neutron sub-shells (^{16}O, ^{22}O, ^{24}O, and ^{28}O) as a function of the neutron number. We assume a normal filling of the orbitals with the order determined by single-particle energies with respect to the core nucleus (a Hartree-Fock approximation). The ESPEs are thus represented by straight segments, whose slopes are given by the corresponding centroids of the two-body interaction, as seen from Eq. (2).

In all cases, the starting point is the A-independent single-particle energies from the USDB Hamiltonian, quoted in the previous section. The TBMEs of USDB and of the microscopic effective interactions are scaled as stated above.

While the neutrons fill $0d_{5/2}$, $1s_{1/2}$ and $0d_{3/2}$ orbitals (from ^{16}O to ^{22}O, then to ^{24}O and on to ^{28}O), the ESPEs acquire shifts due to additional increments provided by the respective centroids. Two important features of the phenomenological USDB interaction are easily seen. First, there is the appearance of a relatively large $N = 14$ subshell closure in ^{22}O. Similarly, there is a clear $N = 16$ shell gap in ^{24}O, resulting in the corresponding magic structure of that nucleus.

As seen from Fig. 5(a), the neutron ESPEs obtained from DJ16$_4$ do show the $N = 14$ subshell in ^{22}O, but its $d_{5/2} - s_{1/2}$ gap is not as large as that from USDB [Fig. 5(e)]. This feature was discussed in detail in our previous work [12], where DJ16$_4$ was selected as a potential providing the maximum $N = 14$ subshell gap among a selected set of microscopic interactions. At the same time, we notice that the new interaction DJ16$_6$, obtained in the present work from Daejeon16 at $N_{\max} = 6$, is characterized by a larger $N = 14$ subshell gap [see Fig. 5(b)]. The numerical values of all the $N = 14$ shell gaps in the O isotopes as obtained from various interactions shown in Fig. 5 are summarized in Table III. The evolution of the $N = 14$ shell gap is governed by the difference between $V_{d_{5/2}d_{5/2}}^{T=1}$ and $V_{d_{5/2}s_{1/2}}^{T=1}$ centroids of the TBMEs. The detailed spin-tensor structure of those centroids will be discussed below.

We also note that the spin-orbit splitting between $0d_{3/2}$ and $0d_{5/2}$ ESPEs is somewhat smaller for DJ16$_4$ and DJ16$_6$ compared with USDB (see also Table III). Specifically, at

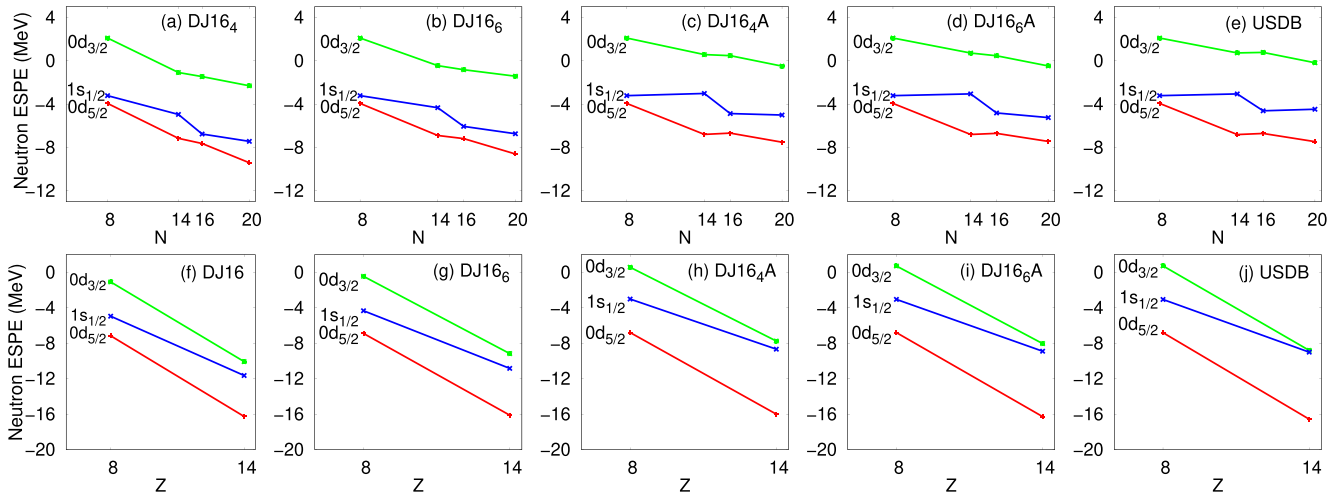

FIG. 5. Variation of neutron ESPEs (a)–(e) in O isotopes with neutron number N (upper row) and (f)–(j) in $N = 14$ isotones (lower row) calculated using the microscopic effective interactions obtained from Daejeon16 and the phenomenological interaction (USDB).

$N = 14$ and $N = 16$, this spin-orbit splitting for DJ16$_6$ is only about 15% smaller than that provided by USDB.

The second visible difference between USDB and both DJ16$_4$ and DJ16$_6$ is related to the magnitude of all slopes of ESPEs in O isotopes: these two DJ16's typically provide a larger negative increment of the centroids with N than those of USDB (see Fig. 5). Since the monopole Hamiltonian provides the major contribution to the nuclear binding, we can immediately conclude that DJ16$_4$ and DJ16$_6$ will result in the overbinding of O isotopes, which we will discuss later. An encouraging trend is seen in the result since the inclusion of additional correlations arising at $N_{\max} = 6$ improves the monopoles compared with USDB, which will reduce the resulting overbinding of O isotopes.

In Ref. [2], the behavior of the ESPEs obtained from microscopic effective interactions, based on a NN potential, was ascribed to the missing 3N forces (see Fig. 2 of that reference). Indeed, the centroids of the microscopic interactions obtained on the basis of NN plus 3N forces show a much better agreement with the centroids of phenomenological interactions [2–4,7]. Daejeon16 is obtained from phase-equivalent transformations of SRG-evolved chiral NN potential at N3LO, which tends to incorporate effects of many-body forces. Thus, it may be that increasing the model space, when progressing from DJ16$_4$ to DJ16$_6$, more completely incorporates the influence of those many-body forces effectively included in Daejeon16 and results in the improved monopole behaviors.

The proton-neutron centroids can be analyzed using the neutron ESPEs in $N = 14$ isotones from ^{22}O to ^{28}Si, i.e., when protons fill the $d_{5/2}$ orbital. The corresponding plots are shown in Figs. 5(f)–5(j). The starting points of these calculations are ESPEs in ^{22}O as obtained by different effective interactions and shown in Figs. 5(a)–5(e). The numerical values of the $N = 14$ shell gaps from the monopole part of the interactions are summarized in Table IV. We notice that in ^{22}O the $N = 14$ subshell gaps given by DJ16$_4$ and DJ16$_6$, except for $d_{3/2}$-$d_{5/2}$, are somewhat smaller than the corresponding gaps from USDB. However, let us concentrate on the evolution of the first subshell gap from ^{22}O towards ^{28}Si, produced by the USDB interaction which increases by 3.82 MeV. DJ16$_4$ results in an increase of 2.41 MeV, while DJ16$_6$ produces an increase of 2.72 MeV. This means that with DJ16$_6$ the difference between the corresponding centroids, $V^{pn}_{d_{5/2}d_{5/2}}$ and $V^{pn}_{s_{1/2}d_{5/2}}$, trends closer to the USDB value.

From Table IV one observes that the spin-orbit splitting between neutron $0d_{3/2}$ and $0d_{5/2}$ states in ^{28}Si stays about the same as in ^{22}O for the both microscopic interactions, as well as for USDB.

Although we have noted an encouraging trend in the monopole properties when moving from DJ16$_4$ to DJ16$_6$, we also note that the gaps and slopes governed by the neutron-neutron centroids are still significantly different from the USDB benchmark. As in our previous study, with further guidance from USDB [Figs. 5(e) and 5(j)], we now perform a few modifications of the DJ16$_6$ centroids to improve agreement with experiment. Namely, we now modify the original DJ16$_6$ centroids by introducing shifts that improve their alignment with USDB centroids as indicated in Table V. The monopole modified interaction is referred to as DJ16$_6$A. In the same table, we show for comparison the modification performed to the previously derived interaction, DJ16$_4$, to get DJ16$_4$A from Ref. [12]. First, we notice that the modifications are mainly of the same type: make the $T = 1$ centroids of DJ16$_6$ more repulsive, which will tend to lessen the overbinding of the O isotopes. The most significant change is again required for $V^{T=1}_{d_{5/2}s_{1/2}}$ to correct the $N = 14$ subshell gap in ^{22}O. The $T = 0$ centroids are little changed. Second, we notice that modifications required for DJ16$_6$ are generally smaller than those applied to DJ16$_4$, with a few exceptions. This is in line with the trend of ESPEs. We distribute monopole modifications evenly among the TBMEs of different J. The TBMEs of the DJ16$_6$A interaction can be found in Table I of the Supplemental Material [22].

TABLE IV. Evolution of the neutron sub-shell shell gaps in $N = 14$ isotones from ^{22}O to ^{28}Si as obtained from the ESPEs of different Hamiltonians.

	Gap $\nu(s_{1/2}-d_{5/2})$ (MeV)			Gap $\nu(d_{3/2}-d_{5/2})$ (MeV)			Gap $\nu(d_{3/2}-s_{1/2})$ (MeV)		
	^{22}O	^{28}Si	Diff	^{22}O	^{28}Si	Diff	^{22}O	^{28}Si	Diff
DJ16$_4$	2.21	4.62	2.41	6.08	6.19	0.11	3.87	1.57	−2.30
DJ16$_6$	2.56	5.28	2.72	6.45	6.95	0.50	3.88	1.67	−2.21
DJ16$_4$A	3.78	7.33	3.55	7.37	8.25	0.88	3.59	0.92	−2.67
DJ16$_6$A	3.75	7.38	3.63	7.52	8.24	0.72	3.77	0.86	−2.91
USDB	3.75	7.57	3.82	7.53	7.77	0.23	3.78	0.20	−3.58

The resulting neutron ESPEs from DJ16$_6$A are shown in Figs. 5(d) and 5(i). As was intended with these modifications, the spherical mean fields from DJ16$_4$A and DJ16$_6$A are close to the mean field provided by USDB. Therefore, the differences between the spectroscopies emerging from modified Daejeon16 effective interactions (DJ16$_4$A, DJ16$_6$A) and the USDB interaction will be mainly related to differences in the other multipole terms of the effective interaction.

IV. COMPARISON WITH EXPERIMENT

A. O isotopes

We begin our discussion of spectroscopic properties with the spectra of the $^{21-24}$O isotopes as obtained from shell-model diagonalization with the microscopic interactions described above. In addition, we include a comparison with results from the IMSRG approach from Ref. [7]. These theoretical results are shown in Fig. 6 in comparison with the experimental spectrum and the spectrum from USDB.

Although the $N = 14$ subshell gap from DJ16$_4$ and DJ16$_6$ is larger than that predicted by other microscopic interactions studied in Ref. [12], it is still not large enough to provide satisfactory spectra when comparing with experiment. This is manifested in low $1/2^+$ and $3/2^+$ states in ^{21}O and the low 2^+_1 state in ^{22}O. Similarly, the lowest $5/2^+$ state in the spectrum of ^{23}O is also lower than the experimental counterpart (Fig. 6). These nuclei have one neutron hole or one particle beyond semimagic ^{22}O. Monopole modifications included in DJ16$_4$A and DJ16$_6$A largely correct these shortcomings and provide closer agreement with experiment.

For comparison, we also show the IMSRG results obtained with the Hamiltonians from Refs. [6,7]. The corresponding spectra are in good agreement with experiment due, in large measure, to the satisfactory $T = 1$ monopole component of the interaction as was discussed in Ref. [12]. With IMSRG, a few low-lying states are positioned slightly higher in energy than their experimental counterparts.

The ground state energies of the O isotopes relative to the ground energy of ^{16}O are shown in Fig. 7. Here, one observes that DJ16$_6$ reduces the overbinding of neutron-rich O isotopes, compared with DJ16$_4$. Furthermore, DJ16$_6$A produces an excellent description of experimental binding energies. The root-mean-square (rms) deviations in experiment versus theory binding energies are summarized in Table VI. Indeed we notice that, among the theoretical cases tabulated, DJ16$_6$A

TABLE V. Centroids (in MeV) of DJ16$_4$ and DJ16$_6$ and the changes ("Diff") which yield the centroids of DJ16$_4$A and DJ16$_6$A, respectively.

	$N_{\max} = 4$			$N_{\max} = 6$		
	DJ16$_4$	DJ16$_4$A	Diff	DJ16$_6$	DJ16$_6$A	Diff
$V^{T=1}_{d_{5/2}d_{5/2}}$	−0.705	−0.625	+0.080	−0.647	−0.627	+0.020
$V^{T=1}_{d_{5/2}s_{1/2}}$	−0.335	+0.015	+0.350	−0.221	+0.008	+0.230
$V^{T=1}_{d_{5/2}d_{3/2}}$	−0.595	−0.295	+0.300	−0.479	−0.269	+0.210
$V^{T=1}_{d_{3/2}s_{1/2}}$	−0.282	−0.082	+0.200	−0.265	−0.165	+0.100
$V^{T=1}_{d_{3/2}d_{3/2}}$	−0.411	−0.411	0	−0.300	−0.400	−0.100
$V^{T=1}_{s_{1/2}s_{1/2}}$	−2.017	−2.017	0	−1.910	−1.910	0
$V^{T=0}_{d_{5/2}d_{5/2}}$	−2.745	−2.825	−0.080	−2.818	−2.918	−0.100
$V^{T=0}_{d_{5/2}s_{1/2}}$	−2.551	−2.451	+0.100	−2.577	−2.527	+0.050
$V^{T=0}_{d_{5/2}d_{3/2}}$	−3.213	−3.213	0	−3.208	−3.408	−0.200
$V^{T=0}_{d_{3/2}s_{1/2}}$	−2.534	−2.534	0	−2.760	−2.760	0
$V^{T=0}_{d_{3/2}d_{3/2}}$	−2.675	−2.675	0	−2.655	−2.655	0
$V^{T=0}_{s_{1/2}s_{1/2}}$	−2.938	−2.938	0	−2.851	−2.851	0

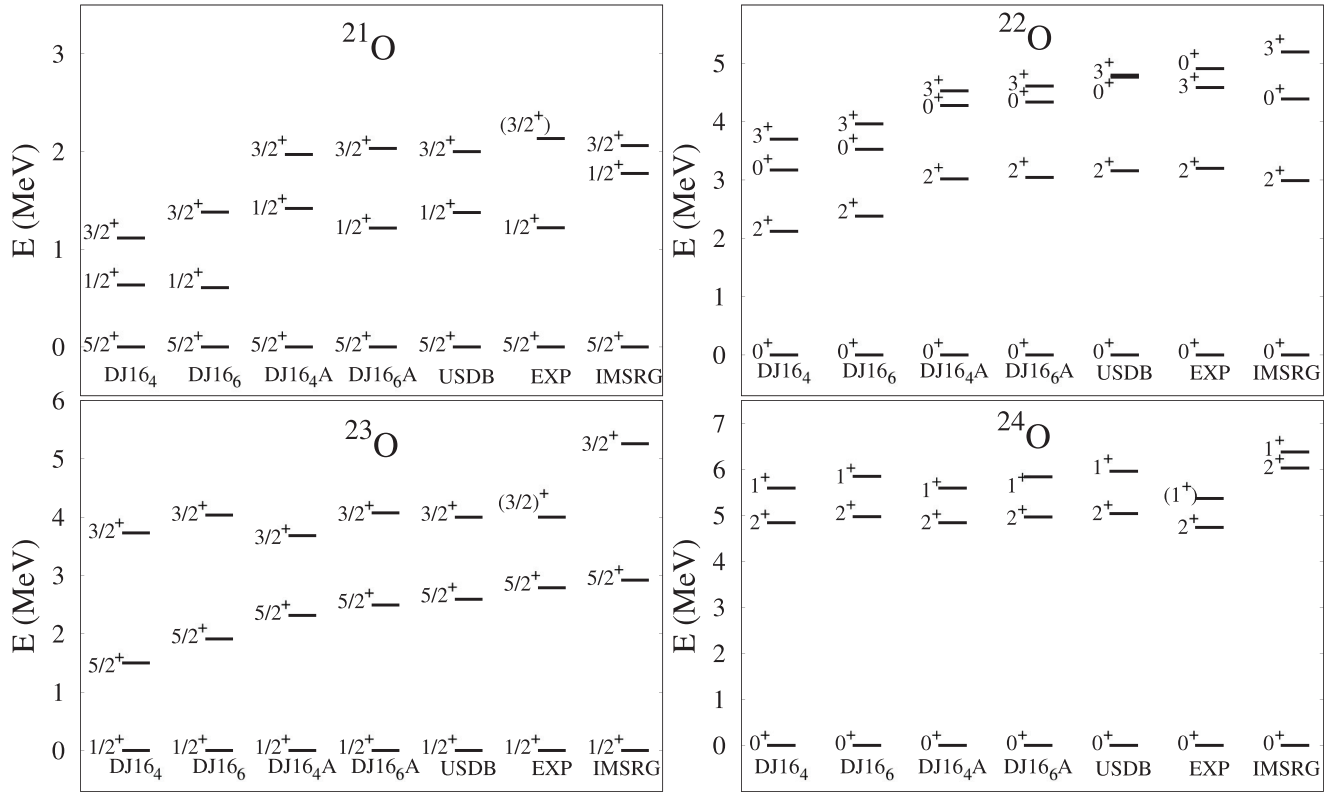

FIG. 6. Experimental low-energy spectrum of $^{21-24}$O in comparison with theoretical results, obtained from USDB and from the microscopic effective interactions. The experimental data are from Ref. [38]. The results labeled "IMSRG" are from Ref. [7].

provides the smallest rms deviation for the binding energy of the O isotopes (column 2 of Table VI).

B. Odd-*A* F isotopes and ^{39}K

The odd-*A* F isotopes are important because, while neutrons are affected by the pairing force, the proton single-particle centroids can provide direct information on the proton-neutron monopoles. In practice, it is difficult to obtain the experimental centroids due to the sparsity and imprecision of available data on the spectroscopic factors. The low-energy theoretical spectra of odd-*A* F isotopes are shown in Fig. 8 in comparison with experiment. In these calculations we introduce DJ16$_6$B, which is DJ16$_6$A with modified quadrupole pairing TBMEs. The idea is to improve a few characteristic spectra, such as ^{25}Mg; see the discussion in Ref. [40]. To this end, we have modified three nondiagonal TBMEs, namely, $\langle d_{5/2}d_{3/2}|V|d_{5/2}s_{1/2}\rangle_{JT}$, $\langle d_{5/2}d_{3/2}|V|d_{3/2}s_{1/2}\rangle_{JT}$, and $\langle d_{5/2}s_{1/2}|V|d_{3/2}s_{1/2}\rangle_{JT}$ with $J = 2$ and $T = 0$ by making them 1.13, 1.83, and 0.45 MeV more repulsive, respectively. The TBMEs of the DJ16$_6$B interaction are given in Table I of the Supplemental Material [22].

When discussing odd-*A* fluorine isotopes, we expect that only in ^{23,25}F the low-lying $5/2^+$, $1/2^+$, and $3/2^+$ states may contain appreciable proton $d_{5/2}$, $s_{1/2}$, and $d_{3/2}$ single-particle components, respectively. In other cases, neutron correlations have more heavily mixed configurations arising from coupling to proton degrees of freedom.

TABLE VI. Root-mean-square deviations (in keV) between experimental and theoretical binding energies of O isotopes and between experimental and theoretical excitation energies of low-lying states of a few *sd*-shell nuclei shown in Figs. 6–10 as obtained from different interactions.

Interaction	BE(O)	$^{21-24}$O	^{19,21,23,25,27}F and ^{39}K	^{22}Na	^{28}Si, ^{32}S	^{24}Mg	^{25}Mg
DJ16$_4$	5960	931	700	429	1146	1096	1314
DJ16$_6$	3671	741	649	336	1015	831	1149
DJ16$_4$A	449	274	285	328	891	806	925
DJ16$_6$A	235	248	308	300	795	781	790
DJ16$_6$B	235	248	388	197	634	696	419
USDB	467	251	437	155	234	313	75
IMSRG	1177	728		445	1497		

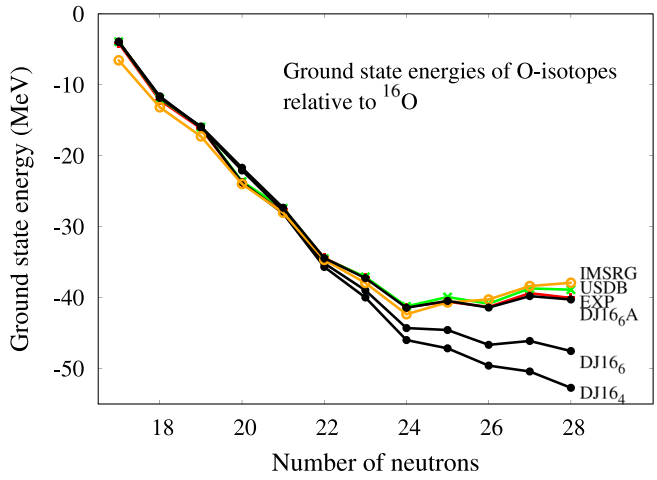

FIG. 7. Experimental ground state energies of O isotopes relative to the ground state energy of ^{16}O, in comparison with theoretical results, obtained from USDB and from the microscopic effective interactions. The experimental data (extrapolations included) are from AME2012 [39]. The results labeled "IMSRG" are from Ref. [7].

The low-lying states of ^{19}F are relatively well-reproduced by all interactions, which is a typical trend for nuclei with a small number of valence particles. In the case of ^{21}F, there is an inversion of the lowest $1/2^+$ and $5/2^+$ states in the spectra obtained by DJ16$_4$ and DJ16$_6$ and other microscopic interactions obtained from various realistic *NN* potentials when compared with experiment or with USDB. One of the possible reasons is the insufficient $N = 14$ shell gap seen in Fig. 5. Modifications made to the monopoles to produce the DJ16$_4$A interaction succeed in yielding the $5/2^+$ ground state, but produce inverted higher lying $3/2^+$ and $9/2^+$ states. DJ16$_6$A provides correct ordering of $3/2^+$ and $9/2^+$, contrary to any other interaction, including USDB, while DJ16$_6$B spoils this ordering of high-lying states although clearly improves splitting of low-lying $5/2^+$ and $1/2^+$.

The small $N = 14$ subshell gap in ^{22}O, as obtained from the valence-space effective interactions DJ16$_4$ and DJ16$_6$, manifests itself in a downward shift of the excitation spectrum of ^{23}F relative to experiment, shown in Fig. 8. In particular, the first $1/2^+$ and $3/2^+$ states, which contain large components of proton $s_{1/2}$ and $d_{3/2}$ single-particle states, are too low with respect to the experimental data and to the USDB calculation. Similarly, the small gap $N = 14$ gap will lead to the low $1/2^+$ state in ^{25}F. Again, we see that these features are improved from DJ16$_4$ to DJ16$_6$, and that there is a rather good agreement between DJ16$_4$A, DJ16$_6$A, USDB, and experiment. It is interesting that the position of the $1/2^+$ first excited state in ^{27}F, observed in Ref. [42], is better described by DJ16$_6$, DJ16$_4$A, and DJ16$_6$A than by USDB. We can make the same remark for DJ16$_6$B: while being slightly better than DJ16$_4$A and DJ16$_6$A for light fluorine isotopes, it fails to produce a sufficiently low $1/2^+$ state in ^{27}F. Since an elevated position of this state is common to both DJ16$_6$B and USDB, one infers a connection with quadrupole pairing.

Finally, to see what happens as the *sd* shell becomes almost filled, we present the spectrum of ^{39}K, which may shed additional light on the evolution of the nuclear mean field. The experimental spectrum of ^{39}K (Fig. 8) shows the centroids of the single-particle states, as extracted from Ref. [43]. They can be directly compared to the theory. Although the DJ16$_4$ and DJ16$_6$ interactions show that the $1/2^+$ state is slightly elevated, there is in general a robust agreement with the experiment. Since the spectrum of ^{39}K is sensitive only to the monopole part of the *sd*-shell Hamiltonian, DJ16$_6$B produces exactly the same spectrum as DJ16$_6$A and, hence, we do not show it in the figure.

The rms deviations of the excitation energies relative to experiment for the odd-*A* fluorine isotopes and ^{39}K can be found in the fourth column of Table VI. Note that, among other microscopic interactions, DJ16$_4$A produces the smallest rms deviation for this particular group of six nuclei.

C. ^{22}Na

The case of ^{22}Na with three protons and three neutrons in the valence space is considered to be an important benchmark of the 3*N* forces [44]. As seen from Fig. 9, the $T = 0$ spectra from DJ16-family of valence-space effective interactions provide robust overall agreement with experiment, although the details are not fully reproduced. The crucial thing is that the ground state is correctly found to be 3^+ in all theoretical cases except IMSRG, with the splitting between 1^+ and 3^+ state being in the best agreement for DJ16$_6$B. Indeed, besides the improvement in monopole properties, the latter suggests that further improvements will accrue with modified quadrupole pairing TBMEs.

The rms deviations between theory and experiment for excitation energies of ^{22}Na are given in Table VI (the fifth column). A continuous reduction of the rms deviations is evident from DJ16$_4$ to DJ16$_6$ and from DJ16$_4$A to DJ16$_6$A. Thus, expanding our NCSM basis space and including the monopole modifications which, combined, results in DJ16$_6$A, leads to an essential decrease of the rms deviation (from 439 to 300 keV). It is also noteworthy that DJ16$_6$B is characterized by an even smaller rms deviation (197 keV), approaching the USDB value (155 keV) where the main difference in rms values arises from the locations of their 5^+ states.

V. QUADRUPOLE PROPERTIES AND Mg ISOTOPES

To characterize the proton-neutron quadrupole component of the microscopic interactions, we consider the spectrum of a well-known *sd*-shell rotor, ^{24}Mg; see Fig. 10. We remark that the ground-state band is relatively well described by all interactions presented. The DJ16$_4$ and DJ16$_6$ interactions produce a somewhat lower lying and slightly more stretched γ band, as compared to experiment and to the USDB result. This feature is corrected partially by the monopole modifications. We also find that there is a further improvement in the location of the γ band with DJ16$_6$B.

In addition, we have calculated a neighboring nucleus, ^{25}Mg, with results presented in Fig. 11 and compared with experiment. This nucleus is known to be a difficult case for microscopic interactions. Indeed, a microscopic theory

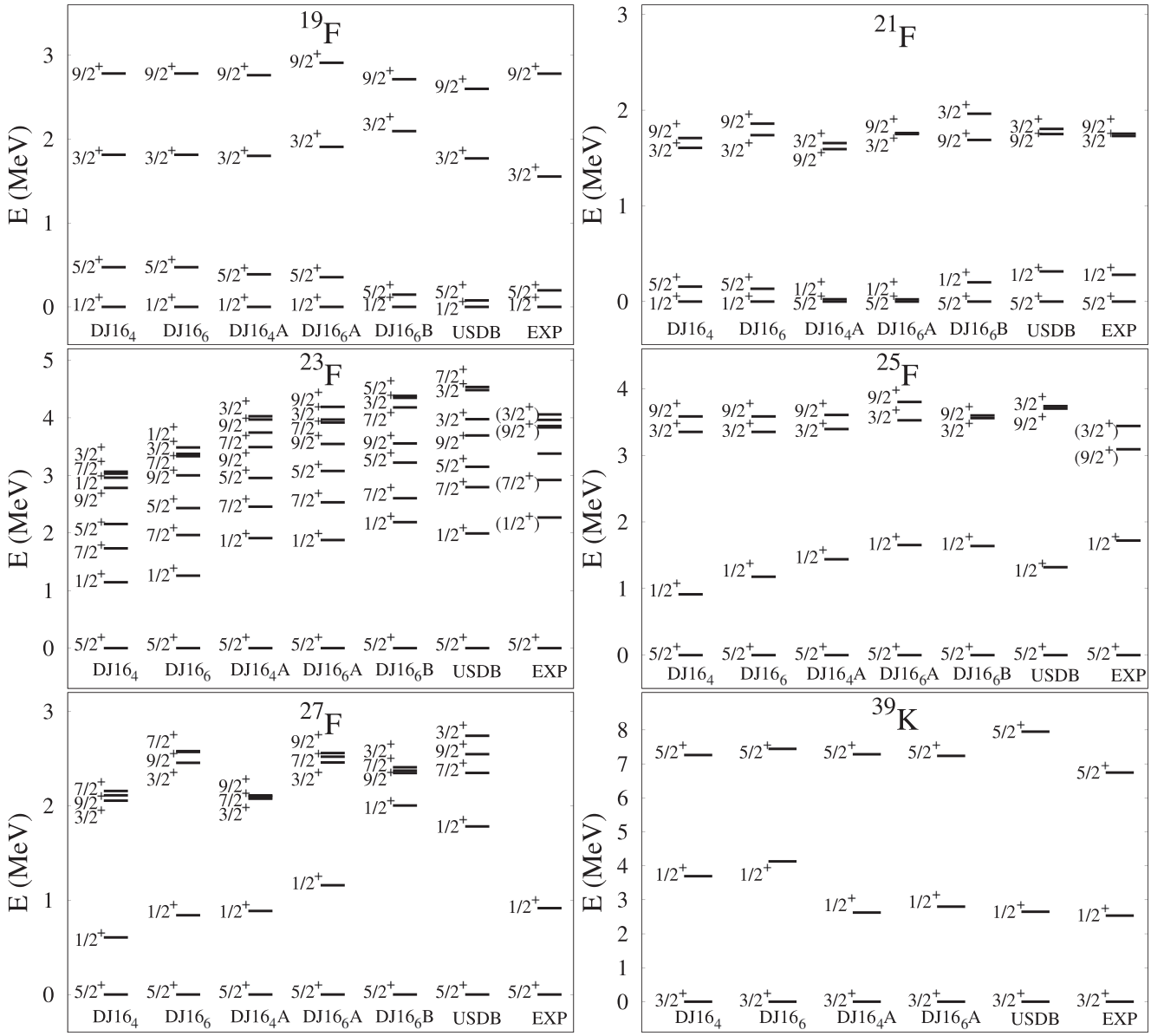

FIG. 8. Low-energy spectra of odd-A $^{19-27}$F and ^{39}K, obtained from USDB and microscopic effective interactions based on Daejeon16, in comparison with the experimental data on positive-parity states from Refs. [38,41,42]. For ^{39}K, we show experimentally deduced centroids from Ref. [43].

prefers to describe this nucleus as a neutron coupled to the well-deformed core of ^{24}Mg and, therefore, we see at low energies a typical rotational band from $1/2^+$, $3/2^+$, and $5/2^+$. This is not at all what is observed experimentally where, instead, a $5/2^+$ ground state is determined. The USDB interaction is known to cope with this feature by a strong quadrupole pairing. Monopole corrections proposed by DJ16$_4$A and DJ16$_6$A are seen to be in line with these changes, since we notice a lowering of the $5/2^+$ state. Furthermore, DJ16$_6$B demonstrates that increasing the amount of quadrupole pairing finally produces a $5/2^+$ ground state, although it is not well separated from the first excited state $1/2^+$.

VI. CONCLUSIONS AND SUMMARY

In the present work we compared the general properties of the new microscopic effective *sd* shell interactions obtained from the NCSM wave functions via the OLS transformation. The NCSM calculations were performed using the Daejeon16 *NN* potential in the model space truncated at $N_{\max} = 6$ with a fixed value of $\hbar\Omega = 14$ MeV.

Since the theoretical single-particle energies show major deficiencies when compared with empirical values, we adopted the empirical single-particle energies for these investigations. In addition, to accommodate the expected dependence of the mean-field with increasing A, we used the USDB scaling of the TBMEs.

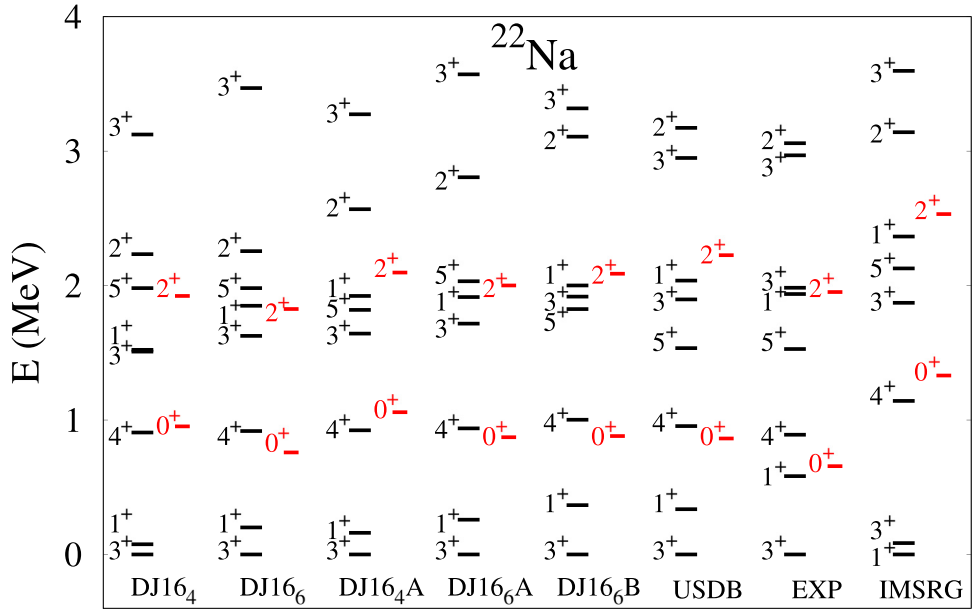

FIG. 9. Low-energy spectrum of ^{22}Na obtained from USDB and microscopic effective interactions, in comparison with the experimental data on positive-parity states from Ref. [38]. $T = 0$ states are shown in black, while $T = 1$ states are plotted in red.

The monopole components of the derived microscopic effective interaction are compared to those of the phenomenological USDB interaction and to an earlier effective interaction constructed in a similar manner from NCSM calculations with Daejeon16 at $N_{\max} = 4$ [12]. We obtain a general improvement in the monopole evolution and in the binding energy of O isotopes using a larger model space. The improving trend suggests the need for even larger model spaces.

To improve the description of the data, we propose minimal modifications to the centroids of the derived effective interaction, with the aim to reproduce the $N = 14$ shell gap, important for the O isotopes. The monopole-modified interaction (DJ16$_6$A) provides excellent agreement for binding energies of the O isotopes and greatly improves the excitation spectra of the oxygen chain as well as the odd-A F isotopes. Furthermore, we show that modification of the quadrupole pairing helps to reproduce the spectrum of ^{25}Mg, for example. Extended calculations through the *sd* shell are summarized in Supplemental Material [22].

We performed calculations of rms deviations based on 256 states in nuclei discussed in this work. Only those

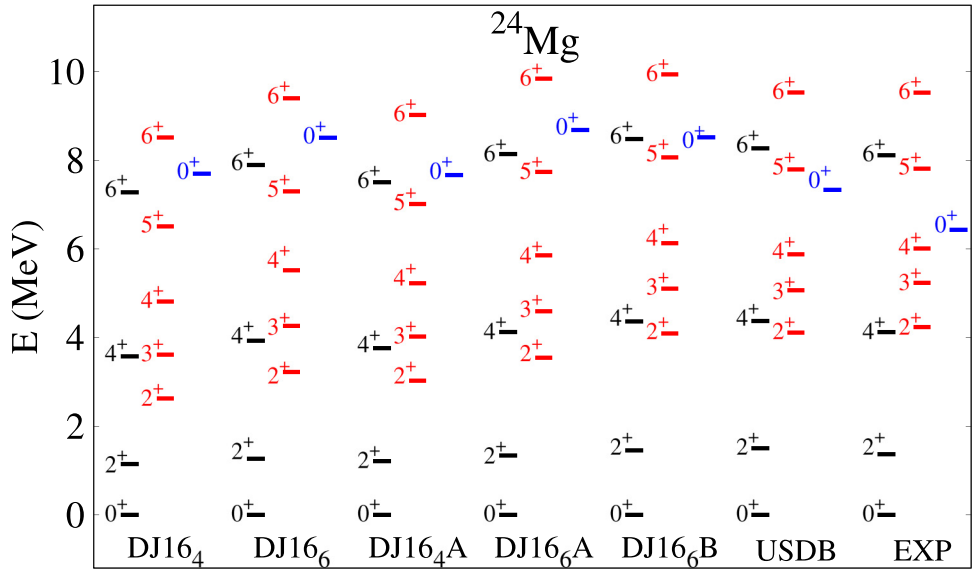

FIG. 10. Low-energy spectrum of ^{24}Mg obtained from USDB and microscopic effective interactions, in comparison with the experimental data on positive-parity states from Ref. [38]. Different rotational bands are distinguished by color.

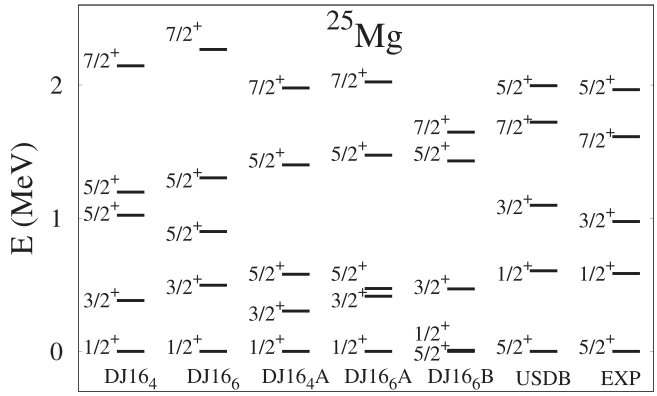

FIG. 11. Low-energy spectrum of ^{25}Mg obtained from USDB and microscopic effective interactions, in comparison with the experimental data on positive-parity states from Ref. [38].

experimental states were retained for which we can reasonably identify a theoretical counterpart. A comparison of rms deviations resulting from various effective interactions in the valence *sd* shell discussed above is presented in Table VI above and in Fig. 12 of the Supplemental Material [22].

As may be expected, the USDB interaction provides a better overall description of experimental data as compared to the derived interactions. Theoretical uncertainties in our approach arise from the truncation of the NCSM space and the uncertainty in the NCSM state selection, as well as from deficiencies of the Daejeon16 *NN* interaction in describing the *sd*-shell nuclei. Indeed, this is the first study of the convergence issue and we notice that the convergence trend of excitation spectra dominated by $N = 0$ components is encouraging though the complete convergence is not achieved. The exceptions are the four highest in energy states which are not converged yet and this may result in an uncertainty. Next, we notice that at $N_{\max} = 6$ it becomes difficult to select the full set of $(N = 0)$-dominated states for the OLS transformation, since high lying states become more fragmented due to the higher level densities and mixtures with intruder configurations. This limits the work at the optimal $\hbar\Omega$ value and may hamper the use of larger $N_{\max}$ model spaces.

Further improvements may come from an updated *NN* interaction, from an alternative state selection procedure and from an increase of the NCSM space. The work on adjustment of the Daejeon16 *NN* interaction by phase-equivalent transformations to improve the *ab initio* description of nuclei at the beginning of the *sd* shell is in progress.

ACKNOWLEDGMENTS

N.A.S. and Z.L. acknowledge the financial support of CNRS/IN2P3, France, via ENFIA and ABI-CONFI Master projects. The work was supported by the Rare Isotope Science Project of Institute for Basic Science funded by Ministry of Science and ICT and National Research Foundation of Korea (Project No. 2013M7A1A1075764). This work was in part supported by the Institute for Basic Science, Korea (Grant No. IBS-R031-D1). This work was supported in part by the U.S. Department of Energy (DOE) under Grants No. DE-SC0018223 (SciDAC-4/NUCLEI), No. DE-SC0023495 (SciDAC-5/NUCLEI), and No. DE-SC0023692. This research used resources of the National Energy Research Scientific Computing Center (NERSC), a US Department of Energy Office of Science User Facility located at Lawrence Berkeley National Laboratory, operated under Contract No. DE-AC02-05CH11231 using NERSC Award No. NP-ERCAP0020944, and also by the National Supercomputing Center with supercomputing resources including technical support (Grant No. KSC-2020-CRE-0027). The work was supported by the JSPS Grant-in-Aid for Scientific Research (S) under Grant No. 20H05648. The work was partly supported by France-Korea Particle Physics Network via a project ABI-SMNS. N.A.S. and A.M.S. thank the Institute for Basic Science, Daejeon, for hospitality and financial support of their visits. The work of A.M.S. is supported by the Russian Foundation for Basic Research under Grant No. 20-02-00357. A.M.S. also thanks the University of Bordeaux for hospitality and financial support of his visit to CENBG (LP2IB) where a part of this work was done.

[1] M. Hjorth-Jensen, T. T. S. Kuo, and E. Osnes, Phys. Rep. **261**, 125 (1995).
[2] T. Otsuka, T. Suzuki, J. D. Holt, A. Schwenk, and Y. Akaishi, Phys. Rev. Lett. **105**, 032501 (2010).
[3] J. D. Holt, T. Otsuka, A. Schwenk, and T. Suzuki, J. Phys. G **39**, 085111 (2012).
[4] T. Fukui, L. De Angelis, Y. Z. Ma, L. Coraggio, A. Gargano, N. Itaco, and F. R. Xu, Phys. Rev. C **98**, 044305 (2018).
[5] S. K. Bogner, H. Hergert, J. D. Holt, A. Schwenk, S. Binder, A. Calci, J. Langhammer, and R. Roth, Phys. Rev. Lett. **113**, 142501 (2014).
[6] S. R. Stroberg, H. Hergert, J. D. Holt, S. K. Bogner, and A. Schwenk, Phys. Rev. C **93**, 051301(R) (2016).
[7] S. R. Stroberg, A. Calci, H. Hergert, J. D. Holt, S. K. Bogner, R. Roth, and A. Schwenk, Phys. Rev. Lett. **118**, 032502 (2017).
[8] G. R. Jansen, J. Engel, G. Hagen, P. Navrátil, and A. Signoracci, Phys. Rev. Lett. **113**, 142502 (2014).
[9] A. F. Lisetskiy, B. R. Barrett, M. K. G. Kruse, P. Navrátil, I. Stetcu, and J. P. Vary, Phys. Rev. C **78**, 044302 (2008).
[10] A. F. Lisetskiy, M. K. G. Kruse, B. R. Barrett, P. Navrátil, I. Stetcu, and J. P. Vary, Phys. Rev. C **80**, 024315 (2009).
[11] E. Dikmen, A. F. Lisetskiy, B. R. Barrett, P. Maris, A. M. Shirokov, and J. P. Vary, Phys. Rev. C **91**, 064301 (2015).
[12] N. A. Smirnova, B. R. Barrett, Y. Kim, I. J. Shin, A. M. Shirokov, E. Dikmen, P. Maris, and J. P. Vary, Phys. Rev. C **100**, 054329 (2019).
[13] B. A. Brown and B. H. Wildenthal, Annu. Rev. Nucl. Part. Sci. **38**, 29 (1988).
[14] B. A. Brown and W. A. Richter, Phys. Rev. C **74**, 034315 (2006).

[15] A. Poves, J. Sanchez-Solano, E. Caurier, and F. Nowacki, Nucl. Phys. A **694**, 157 (2001).
[16] M. Honma, T. Otsuka, B. A. Brown, and T. Mizusaki, Phys. Rev. C **69**, 034335 (2004).
[17] D. R. Entem and R. Machleidt, Phys. Rev. C **68**, 041001(R) (2003).
[18] A. M. Shirokov, J. P. Vary, A. I. Mazur, and T. A. Weber, Phys. Lett. B **644**, 33 (2007).
[19] A. M. Shirokov, I. J. Shin, Y. Kim, M. Sosonkina, P. Maris, and J. P. Vary, Phys. Lett. B **761**, 87 (2016).
[20] P. Choudhary and P. C. Srivastava, Nucl. Phys. A **1033**, 122629 (2023).
[21] Z. Li, N. Smirnova, A. M. Shirokov, I. J. Shin, B. R. Barrett, P. Maris, and J. P. Vary, arXiv:2205.15939.
[22] See Supplemental Material at http://link.aps.org/supplemental/10.1103/PhysRevC.110.034306 for TBMEs and spectra of sd-shell nuclei.
[23] D. H. Gloekner and D. R. Lawson, Phys. Lett. B **53**, 313 (1974).
[24] P. Sternberg, E. G. Ng, C. Yang, P. Maris, J. P. Vary, M. Sosonkina, and H. V. Le, in *SC '08: Proceedings of the 2008 ACM/IEEE Conference on Supercomputing, Austin, 15–21 November 2008* (IEEE, Piscataway, NJ, 2008).
[25] P. Maris, M. Sosonkina, J. P. Vary, E. G. Ng, and C. Yang, in *Procedia Computer Science, ICCS 2010* (Elsevier, Amsterdam, 2010), p. 97.
[26] H. M. Aktulga, C. Yang, E. G. Ng, P. Maris, and J. P. Vary, in *Euro-Par 2012 Parallel Processing, 18th International Conference, Rhodes, August 2012*, edited by C. Kaklamanis, T. Papatheodorou, and P. G. Spirakis, Lecture Notes in Computer Science (Springer, Heidelberg, 2012), Vol. 7484, p. 830.
[27] H. M. Aktulga, C. Yan, E. G. Ng, P. Maris, and J. P. Vary, Concurr. Comput. Pract. Exper. **26**, 2631 (2014).
[28] M. Shao, H. Aktulga, C. Yang, E. G. Ng, P. Maris, and J. P. Vary, Comput. Phys. Commun. **222**, 1 (2018).
[29] B. R. Barrett, P. Navrátil, and J. P. Vary, Prog. Part. Nucl. Phys. **69**, 131 (2013).
[30] P. Maris, J. P. Vary, and A. M. Shirokov, Phys. Rev. C **79**, 014308 (2009).
[31] M. W. Kirson, Nucl. Phys. A **781**, 350 (2007).
[32] https://github.com/nadya-smirnova/Nmax6.
[33] R. K. Bansal and J. B. French, Phys. Lett. **11**, 145 (1964).
[34] A. Poves and A. P. Zuker, Phys. Rep. **70**, 235 (1981).
[35] A. P. Zuker and M. Dufour, arXiv:nucl-th/9505012.
[36] T. Otsuka, M. Honma, T. Mizusaki, N. Shimizu, and Y. Utsuno, Prog. Part. Nucl. Phys. **47**, 319 (2001).
[37] P. Kumar, K. Jha, P. Raina, and P. P. Singh, Nucl. Phys. A **983**, 210 (2019).
[38] NNDC, http://www.nndc.bnl.gov.
[39] G. Audi, F. G. Kondev, M. Wang, B. Pfeiffer, X. Sun, J. Blachot, and M. MacCormick, Chin. Phys. C **36**, 1157 (2012).
[40] M. Dufour and A. P. Zuker, Phys. Rev. C **54**, 1641 (1996).
[41] M. Vandebrouck *et al.* (R3B collaboration), Phys. Rev. C **96**, 054305 (2017).
[42] P. Doornenbal, H. Scheit, S. Takeuchi, Y. Utsuno, N. Aoi, K. Li, M. Matsushita, D. Steppenbeck, H. Wang, H. Baba *et al.*, Phys. Rev. C **95**, 041301(R) (2017).
[43] P. Doll, G. J. Wagner, K. T. Knöpfle, and G. Mairle, Nucl. Phys. A **263**, 210 (1976).
[44] A. P. Zuker, Phys. Rev. Lett. **90**, 042502 (2003).